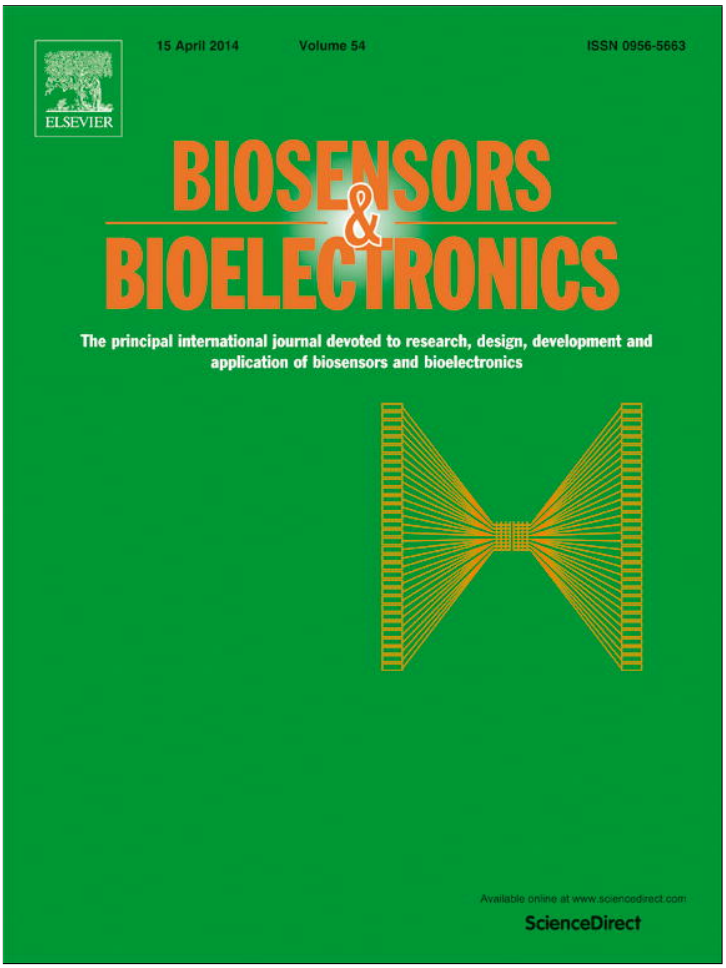

Biosensors and Bioelectronics 54 (2014) 534–540

Contents lists available at ScienceDirect

Biosensors and Bioelectronics

journal homepage: www.elsevier.com/locate/bios

Manganese cobaltite/polypyrrole nanocomposite-based air-cathode for sustainable power generation in the single-chambered microbial fuel cells ☆

Santimoy Khilari [a], Soumya Pandit [b], Debabrata Das [b], Debabrata Pradhan [a,*]

[a] Materials Science Centre, Indian Institute of Technology, Kharagpur 721302, W.B., India
[b] Department of Biotechnology, Indian Institute of Technology, Kharagpur 721302, W.B., India

ARTICLE INFO

Article history:
Received 9 October 2013
Accepted 13 November 2013
Available online 23 November 2013

Keywords:
Microbial fuel cells
Nanorods
Air-cathode
Manganese cobaltite
Polypyrrole

ABSTRACT

Manganese cobaltite nanorods ($MnCo_2O_4$ NRs) were prepared and tested as potential air-cathode catalyst for the single-chambered microbial fuel cells (sMFC). The power generation of sMFC increases with $MnCo_2O_4$ NRs loading to the cathode. The Polypyrrole (PPy) and Vulcan XC were used as conducting support to the $MnCo_2O_4$ NRs to form composites either by *in situ* or by mechanical mixing in the cathode fabrication. The cyclic voltammetry, linear sweep voltammetry and electrochemical impedance studies reveal that the *in situ*-$MnCo_2O_4$ NRs/PPy composite has higher catalytic activity than that of mechanically mixed-$MnCo_2O_4$NRs/PPy composite because of higher interfacial contact between $MnCo_2O_4$ NRs and PPy. The maximum volumetric power density with *in situ*-$MnCo_2O_4$ NRs/PPy, mechanically mixed-$MnCo_2O_4$ NRs/PPy, $MnCo_2O_4$ NRs/Vulcan XC and catalyst-free (only Vulcan XC) cathode was measured to be 6.11, 5.05, 4.22, and 1.77 W/m^3, respectively, in the sMFC. This suggests that PPy is not only a better conducting support than that of conventionally used Vulcan XC but also the cathode composite fabrication process is important for enhanced performance. The synergetic effect of $MnCo_2O_4$ NRs and PPy was found to play an important role for the improved energy recovery and it could be applied as an efficient and inexpensive cathode catalyst for the sMFC.

1. Introduction

Air-cathode microbial fuel cells (MFC) draw much attention of researchers in recent years for the sustainable electricity generation from biodegradable wastes by utilizing electrochemically active bacteria (EAB) (Sevda et al., 2013; Raghavulu et al., 2012). A notable progress has been made on air-cathode MFC design with various engineering approaches (Sevda et al., 2013; Zhang et al., 2011). In order to minimize the internal resistance of air-cathode MFC, various membrane/cloth cathode assemblies (MCAs/CCAs) were developed (Li et al., 2011; Luo et al., 2013). However it has been observed that the performance of MFC is majorly limited by the cathode. Thus the cathode materials and their design are the most challenging aspects for developing an efficient MFC (Pandit et al., 2012). The sluggish oxygen reduction reaction (ORR), increased internal resistance due to hot-pressing of MCAs, and expensive manufacturing costs of MCAs are the important factors which restrict the practical application of MFC (Kim et al., 2007; Rismani-Yazdi et al., 2008). In order to accelerate ORR, a number of electroactive catalysts have been employed. The incorporation of noble metals catalysts such as Pt, Pd, Au, and Ag on cathode considerably decreases the activation energy barrier and improve the ORR kinetics (Zhou et al., 2011; Carpenter et al., 2012; Guo and Sun, 2012). However, the high cost and catalyst poisoning restrict their commercialization. The transition metals, metal oxides and metal complexes were tested as alternate low-cost ORR catalyst to Pt with limited success (Zhou et al., 2011; Ahmed et al., 2012; Wang, L. et al., 2011; Wang, S. et al., 2011; Roche et al., 2009; Zhao et al., 2005).

Further to avoid the bottlenecks associated with hot-pressing process, researchers have employed different means of fabricating MCAs. In particular, Zuo et al. developed a tubular MCA by coating a tubular ultrafiltration membrane with graphite paint and non-precious metal (Zuo et al., 2007). Zhuang et al. constructed a low-cost membrane-less CCA by coating a canvas cloth with nickel-based or graphite-based paint and MnO_2 (Zhuang et al., 2009). Recently, mixed valence transition metal oxides with spinel structures of formula AB_2O_4 attract attention as electrocatalysts for ORR due to their conducting/semiconducting nature (Xu et al., 2012;

* Corresponding author. Tel.: +91 3222 281798; fax: +91 3222 282274.
E-mail address: deb@matsc.iitkgp.ernet.in (D. Pradhan).

0956-5663/$ - see front matter © 2013 Elsevier B.V. All rights reserved.
http://dx.doi.org/10.1016/j.bios.2013.11.044

Wu et al., 2012). The spinels with two different 3d-metal ions at A and B are reported to show improved catalytic activity, selectivity, stability and resistance to poisoning in a number of catalytic/electrocatalytic processes, such as ORR, and oxidation of CO and hydrocarbons (Hamdani et al., 2010; Liang et al., 2012). Among the transition metal spinels, partially substituted cobalt spinel has been studied extensively as electrocatalyst because of its low cost, simple preparation and high stability. Manganese cobaltite ($Mn_xCo_{3-x}O_4$) has been used as ORR catalyst because of its ability to provide donor–acceptor chemisorption sites for the reversible adsorption of oxygen for ORR (Restovic et al., 2002). But poor electrical conductivity is a major drawback of spinel which reduces the electrochemical performance. Therefore, conducting support such as activated carbon has been used to improve its electrochemical activity. Polypyrrole (PPy) is a well-known conducting polymer with good conductivity and stability along with easy preparation (Yuan et al., 2013). Recently, PPy has been used as efficient catalyst support in several electrochemical processes (Mohana Reddy et al., 2008). The unique electronic structure of PPy reduces the ORR activation energy by enhancing oxygen adsorption on its surface (Khomenko et al., 2005). Thus the combination of manganese cobaltite and PPy can be a better performing ORR catalyst for the MFC.

In the present study, we focused on three important aspects of the air-cathode electrode. First, the as-synthesized manganese cobaltite nanorods ($MnCo_2O_4$ NRs) supported on PPy matrix has been evaluated as potential cathode material for the sMFC and its performance is compared with benchmark Pt/C. Second, the role of PPy as a catalyst support is compared with traditional Vulcan XC in the sMFC. Finally, the effect of blending technique (mechanical mixing *vs. in situ* blending) of catalyst dispersion in the PPy support matrix is studied.

2. Material and methods

2.1. Chemicals

Pyrrole (99%) was obtained from Sigma Aldrich. Manganese chloride ($MnCl_2 \cdot 4H_2O$), cobalt chloride ($CoCl_2 \cdot 6H_2O$), hydrochloric acid (HCl) (35% v/v), ammonium fluoride (NH_4F), urea ($CO(NH_2)_2$), ammonium persulfate ($(NH_4)_2S_2O_8$), cetyltrimethylammonium bromide (CTAB) and all other required chemicals were purchased from Merck (India) and used without further purification.

2.2. Synthesis of $MnCo_2O_4$ NRs and PPy

$MnCo_2O_4$ NRs were synthesized using a simple template-free hydrothermal process followed by calcination. In a typical synthesis, 10 mL of each 0.1 M $MnCl_2 \cdot 4H_2O$, 0.2 M $CoCl_2 \cdot 6H_2O$, 0.6 M $CO(NH_2)_2$ and 0.2 M NH_4F solutions were mixed one by one with continuous stirring. The resulting mixture was then transferred to a 50 mL Teflon-lined stainless steel autoclave and heated at 130 °C for 6 h in a muffle furnace. Subsequently the furnace was cooled to room temperature naturally and precipitate formed inside the container was collected by centrifuge. The precipitate was first washed with distilled water several times followed by ethanol and dried at 70 °C for 6 h. The dried precipitate was calcined at 400 °C in air for 2 h.

PPy was synthesized by oxidative polymerization of pyrrole at room temperature. In a typical polymerization, 364 mg CTAB was dispersed in 80 mL 1 M HCl by sonication. Then 0.14 mL of pyrrole monomer was added to the solution with constant stirring. Polymerization was initiated by adding 20 mL 1 M HCl containing 570 mg $(NH_4)_2S_2O_8$. The resulting mixture was stirred for 12 h. The product formed was centrifuged and washed with 1 M HCl, distilled water and ethanol. Finally, washed precipitate was dried at 60 °C for 6 h.

2.3. Synthesis of $MnCo_2O_4$ NRs/PPy and $MnCo_2O_4$ NRs/Vulcan XC composite

$MnCo_2O_4$ NRs/PPy composite was synthesized either *in situ* or by mechanical mixing. The *in situ*-$MnCo_2O_4$ NRs/PPy was synthesized by polymerization of pyrrole in presence of $MnCo_2O_4$ NRs. 100 mg of $MnCo_2O_4$ NRs was dispersed in 80 mL 1 M HCl and sonicated for 20 min. Then 0.14 mL monomer solution was added and stirred for another 30 min. Rest of the procedure remain same as the PPy synthesis. The mechanically mixed $MnCo_2O_4$ NRs/PPy (m-$MnCo_2O_4$ NRs/PPy) composite was prepared by ultrasonically mixing $MnCo_2O_4$ NRs (100 mg) with PPy (150 mg) in acetone and 10 wt% Nafion™ suspensions (Aldrich). The $MnCo_2O_4$ NRs/Vulcan XC composite was prepared in the same way as that of m-$MnCo_2O_4$ NRs/PPy by replacing PPy with Vulcan XC.

The details on catalyst characterization, MCA preparation, and MFC operation are presented in the Supplementary material (SI).

3. Results and discussion

3.1. Morphology and crystal structure of the catalysts

The surface morphology of the as-synthesized samples was analyzed by the field emission scanning electron microscope (FE-SEM) and shown in Fig. 1. Fig. 1(a) shows the flower-like spherical structures with diameter 3–6.5 μm. The magnified FE-SEM image [inset Fig. 1(a)] clearly indicates that these flower-like structures are assembled of $MnCo_2O_4$ NRs with an average diameter of ~65 nm and length 0.6–1 μm. The magnified images reveal that $MnCo_2O_4$ NRs are consisted of interlinked particles forming one-dimensional nanostructure, as confirmed by transmission electron microscopy (TEM). The FE-SEM image [Fig. 1(b)] of as-synthesized PPy shows 80–160 nm diameter agglomerated particles.

Microstructural analysis of as-synthesized samples was carried out by the TEM. Fig. 1(c) represents a TEM image of $MnCo_2O_4$ NRs with 30–80 nm diameter matching FE-SEM result. It clearly reveals that NRs are formed by regular interconnection of nanoparticles of size < 50 nm. A lattice resolved high-resolution TEM (HRTEM) image [inset Fig. 1(c)] shows an average d-spacing of 0.465 nm corresponding to (111) planes and crystalline nature of particles. Fig. 1(d) displays a TEM image of as-synthesized PPy showing agglomeration of spherical particles of size 90–200 nm. The TEM images of *in situ*-$MnCo_2O_4$ NRs/PPy composite [Fig. 1(e)] show the uniform distribution of $MnCo_2O_4$ NRs in the PPy matrix and $MnCo_2O_4$ NRs are coated well with PPy. However, such well dispersion of $MnCo_2O_4$ NRs in the PPy matrix was not found in the m-$MnCo_2O_4$ NRs/PPy composite as shown in Fig. 1(f). The crystal structure of as-synthesized $MnCo_2O_4$ NRs, PPy and their composites was further analyzed by X-ray diffraction and presented in Fig. S1 of Supporting material (SI).

3.2. Electrochemical ORR activity and charge transport property of composite electrodes

Electrocatalytic activity towards ORR was evaluated by cyclic voltammetry (CV), linear sweep voltammetry (LSV) and electrochemical impedance spectroscopy (EIS). Two different inter-competing mechanisms were proposed for ORR (Lu et al., 2011). Molecular oxygen can be directly reduced to hydroxyl ion by an efficient 4-electron reduction path (Eq. (1)). However the less efficient 2-electron reduction path involves two steps and produced hydrogen peroxide ion (HO_2^-) as an intermediate (Eq. (2))

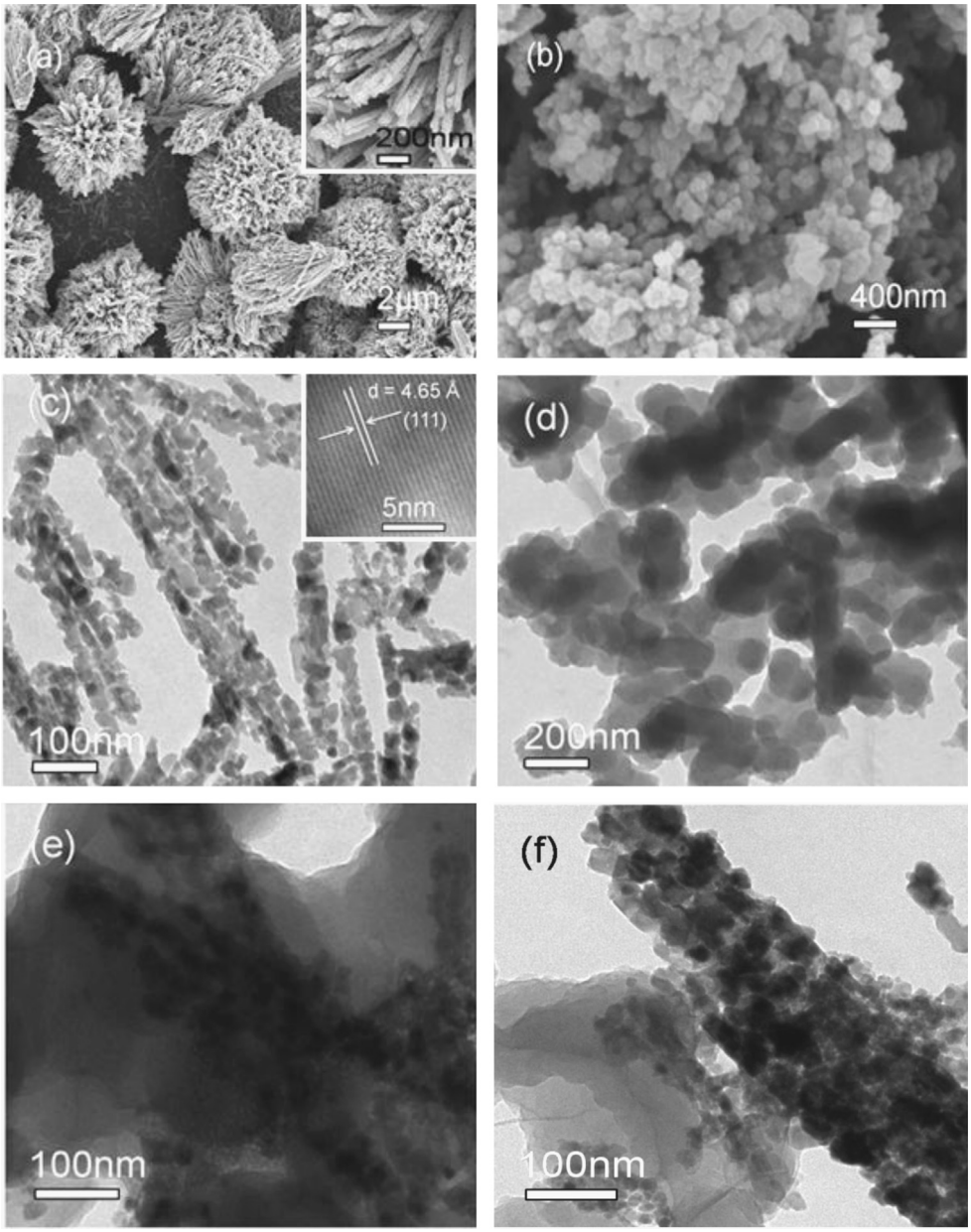

Fig. 1. FE-SEM images of (a) $MnCo_2O_4$ NRs. Inset shows a magnified image, and (b) as-synthesized PPy. TEM images of (c) $MnCo_2O_4$ NRs. Inset shows a lattice image (d) as-synthesized PPy, and (e) *in situ*-$MnCo_2O_4$ NRs/PPy and (f) m-$MnCo_2O_4$ NRs/PPy composites.

which is further reduced by capturing two electrons (Eq. (3a)) or disproportionate in reaction medium (Eq. (3b)). Corrosive HO_2^- ion can reduce the electrochemical activity of cathode and degrade the polymer membrane separator. So, it is desirable to have an ORR catalyst that follows 4-electron pathway with high cell performance and stability.

$$O_2 + 4H^+ + 4e^- \rightarrow 2H_2O \quad (1)$$

$$O_2 + 2H_2O + 2e^- \rightarrow HO_2^- + OH^- \quad (2)$$

$$HO_2^- + H_2O + 2e^- \rightarrow 3OH^- \quad (3a)$$

$$2HO_2^- \rightarrow 4OH^- + O_2 \quad (3b)$$

Fig. 2(a) shows the cyclic voltammogram of different composites in O_2-saturated electrolyte with a cathodic peak at ~0.3 V for ORR which was absent in N_2-saturated electrolyte (Fig. S2, SI). Furthermore, the linear relationship between peak current and square root of scan rate (Fig. S3, SI) indicates the diffusion-controlled process. Fig. 2(a) also shows that the cathodic peak current increased in the order: $MnCo_2O_4$ NRs/Vulcan XC < m-$MnCo_2O_4$ NRs/PPy < *in situ*-$MnCo_2O_4$ NRs/PPy, indicating increase in the ORR rate. In addition, the cathodic peak is shifted to the more positive potential for *in situ*-$MnCo_2O_4$ NRs/PPy composite, suggesting decrease in overpotential for the ORR. The LSV study was performed in O_2-saturated 0.1 M KOH using rotating disk electrode (RDE) to better understand the ORR activity of the as-prepared catalysts. Fig. 2(b) shows the steady state polarization plots of different catalysts at 1600 rpm. The LSV also shows a more positive onset potential and higher ORR current density with Pt/C and *in situ*-$MnCo_2O_4$ NRs/PPy composite than the $MnCo_2O_4$ NRs/Vulcan XC and m-$MnCo_2O_4$ NRs/PPy composites. In addition, the difference in catalytic activity between the Pt/C and *in situ*-$MnCo_2O_4$ NRs/PPy is presented as a difference of half-wave potential ($\Delta E_{1/2}$) in LSV plots (He et al., 2013). The $\Delta E_{1/2}$ is found to be low *i.e.* 50 mV indicating comparable electrocatalytic activity

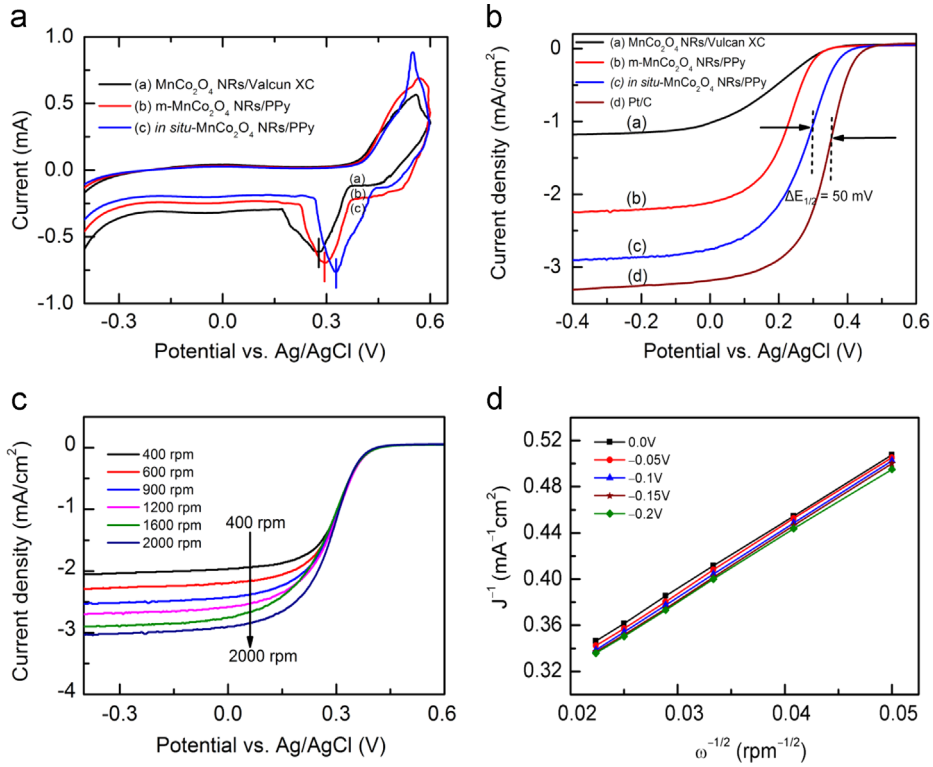

Fig. 2. (a) Cyclic voltammograms recorded at scan rate 10 mV/s with different composite catalysts. (b) Steady state polarization plots of different composites and Pt/C at 1600 rpm, (c) RDE polarization plot of *in situ*-$MnCo_2O_4$ NRs/PPy catalyst obtained with different rotation rates, (d) Koutecky–Levich plots for ORR at *in situ*-$MnCo_2O_4$ NRs/PPy composite coated electrode at different potential. All the voltammograms were recorded *vs.* standard Ag/AgCl in O_2 saturated 0.1 M KOH solution with 10 mV s^{-1} scan rate.

of *in situ*-$MnCo_2O_4$ NRs/PPy with Pt/C. Although the BET surface area of *in situ*-$MnCo_2O_4$ NRs/PPy (46.89 m^2/g) is lower than that of Vulcan XC composite (98.32 m^2/g) and $MnCo_2O_4$ NRs (52.31 m^2/g), the improved catalytic activity of *in situ*-$MnCo_2O_4$ NRs/PPy composite suggests its higher electroactive surface area, better adherence of $MnCo_2O_4$ NRs on the PPy matrix and synergetic effect of the components. Moreover the measured current density increases with *in situ*-$MnCo_2O_4$ NRs/PPy electrode upon increasing RDE speed [Fig. 2(c)]. Three distinct potential region from the LSV plots which affect the ORR are (i) kinetically controlled high potentials region ($E > 0.5$ V), (ii) mixed diffusion-kinetic limited region (0.3–0.4 V), and (iii) diffusion limited region at low potential ($E < 0.0$). The number of electron transfer to each oxygen molecule during ORR can be calculated from Koutecky–Levich (K–L) equation (Wang et al., 2011):

$$1/J = 1/J_L + 1/J_K = 1/B\omega^{1/2} + 1/J_K \quad (4)$$

where J, J_L, J_K are the measured current density, the diffusion-limiting current density and the kinetic-limiting current density, respectively. 'ω' is the rotation speed of RDE. 'B' is determined from the slope of the K–L plots (current density^{-1} *vs.* $\omega^{-1/2}$) using the following Levich equation (Wang et al., 2011)

$$B = 0.2nFC_0(D_0)^{2/3}\upsilon^{-1/6} \quad (5)$$

where 'F' is the Faraday constant (96,485 C/mol), 'D_0' is the diffusion coefficient of oxygen in 0.1 M KOH (1.9×10^{-5} cm^2/s), υ is the kinematic viscosity of the electrolyte (0.01 cm^2/s), and C_0 is the bulk oxygen concentration (1.2×10^{-6} mol/cm^3). The K–L plots obtained with different catalysts (Fig. S4, SI) exhibit linearity. The number of electron transferred (n) during ORR was evaluated using the Levich equation (considering $n = 4$ for Pt/C) and found to be 3.9, 3.7 and 3.5 for *in situ*-$MnCo_2O_4$ NRs/PPy, m-$MnCo_2O_4$ NRs/PPy and $MnCo_2O_4$ NRs/Vulcan XC composites, respectively. This substantiates that ORR at as-prepared composites proceed through 4-electron path. The electron transfer trend (in terms of 'n') of present PPy-based $MnCo_2O_4$ NRs is well within the range of recently reported similar ORR catalysts *i.e.* 3.9 for $MnCo_2O_4$/N-rmGO (Liang et al., 2012) and 3.75 for cobalt oxide coupled nitrogen-doped graphene (He et al., 2013). The J_K values, which suggest about the catalytic activity, were estimated from intercept of the K–L plots (Fig. S4, SI). The J_K for *in situ*-$MnCo_2O_4$ NRs/PPy (4.62 mA/cm^2) is found to be smaller than Pt/C (5.75 mA/cm^2) but significantly higher than m-$MnCo_2O_4$ NRs/PPy (3.12 mA/cm^2) and $MnCo_2O_4$ NRs/Vulcan XC (1.23 mA/cm^2) indicating the importance of *in situ* fabrication of composite. The K–L plots obtained at different potentials with *in situ*-$MnCo_2O_4$ NRs/PPy composite [Fig. 2(d)] shows linearity and near parallelism indicating similar electron transfer process at different potentials. The near parallel K–L plots also suggest the first-order ORR kinetics with respect to O_2 in 0.1 M KOH solution.

EIS has been extensively used to study the interfacial electrochemical properties of an electrode. Nyquist plot, a complex impedance plot between imaginary and real component of impedance provides information about electron-transfer kinetics and diffusion characteristics at the electrode/electrolyte interface. Fig. 3(a) presents the Nyquist plots of bare and catalyst-coated carbon paper electrodes. All the electrodes show semicircle arc-like plot in the high-frequency region followed by straight line in the low-frequency region. The semicircle arc suggests about the charge transfer behavior of an electrode under study. The diameter of the semicircle represents the charge transfer resistance (R_{ct}) at the electrode/electrolyte interface of respective electrode. A significant difference in semicircle diameter has been observed in the impedance plot of different composite electrodes. The R_{ct} values were calculated by fitting the experimental data with an equivalent circuit [Fig. 3(b)] with solution resistance (R_s), R_{ct},

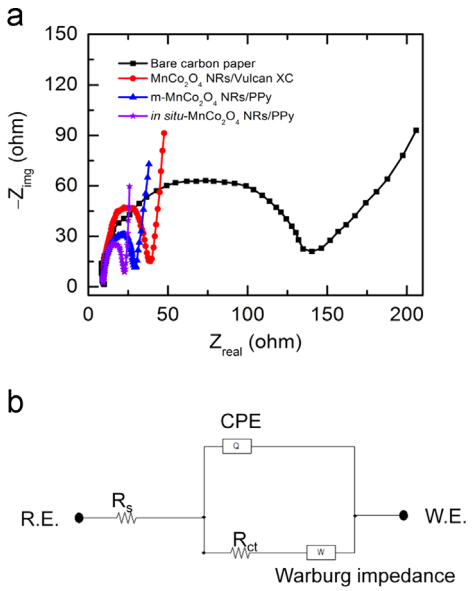

Fig. 3. (a) Nyquist plots of bare, and composites coated carbon paper electrodes in 0.1 M KOH and (b) equivalent circuit used to fit the Nyquist plots.

constant phase element (CPE) and Warburg impedance (Z_w). The R_{ct} values of different electrodes follows the order: bare carbon paper (114.4 Ω) > $MnCo_2O_4$ NRs/Vulcan XC (27.09 Ω) > m-$MnCo_2O_4$ NRs/PPy(22.16 Ω) > *in situ*-$MnCo_2O_4$ NRs/PPy (14.86 Ω). The minimum R_{ct} value obtained from *in situ*-$MnCo_2O_4$ NRs/PPy composite indicates the maximum electron transport, which reduces overpotential and increase the ORR rate supporting the CV and LSV results. The higher ORR kinetics and better charge transport efficiency of *in situ*-$MnCo_2O_4$ NRs/PPy composite is attributed to the higher interfacial contact between $MnCo_2O_4$ NRs and conductive PPy matrix which is not found in the m-$MnCo_2O_4$ NRs/PPy composite (as confirmed by the TEM). Here, PPy act as a bridge between $MnCo_2O_4$ NRs and oxygen for electron transportation. Moreover the PPy matrix has the delocalized π-electron cloud which facilitates adsorption of oxygen and enhances the electron transfer to molecular oxygen (Khomenko et al., 2005; Chen et al., 2012). Similar reduction of R_{ct} was reported with $MnCo_2O_4$/N-rmGO hybrid as compared to mixture of $MnCo_2O_4$ and N-rmGO (Liang et al., 2012). The R_{ct} value of m-$MnCo_2O_4$-NRs/PPy composite is found to be smaller in O_2-saturated electrolyte than N_2-saturated indicating the increase in the electron transfer on oxygen adsorption (SI, Fig. S5) and thereby improvement in ORR.

3.3. *Effect of $MnCo_2O_4$ NRs loading on the electrode potential generation in sMFC*

$MnCo_2O_4$ NRs were loaded in different quantities to Vulcan XC to find its catalytic role in the sMFC. Four different loadings (0.05, 0.1, 0.2 and 0.4 mg/cm^2 $MnCo_2O_4$ NRs) were taken for the MCA fabrication keeping total quantity of catalyst and support constant (0.5 mg/cm^2). The potential generation performance of composite catalysts was compared with the catalyst-free electrode (only Vulcan XC). For the sMFC performance measurement, anaerobic anodic chamber of MFC was fed with lactate-based media using *Shewanella putrefaciens* (ATCC® BAA1097™) as EAB. After inoculation, anode half-cell potential started to decrease owing to the donation of electrons to the anode by EAB and voltage reached at a plateau of about -273 ± 6 mV against an external resistance of 100 Ω for all the sMFC. Under batch mode operation with a feed cycle time of 60 h, all the sMFC took a period of 2 weeks to reach stable condition. Subsequently, slow increase in current was observed with the duration of operation. In all the sMFC, a minimum anode potential reached at -470 ± 6 mV *vs.* Ag/AgCl on 11th days after inoculation. Stable power was generated after six sequential transfer of lactate medium into the chamber of mediator-less sMFC. The anode and cathode potentials as a function of current density were documented to find out the contribution of individual electrode. It was observed that cathode potential determines the power generation in sMFC *i.e.* cathode potentials follow the same trend as power density curves. The corresponding polarization curves of the sMFC, as shown in Fig. S6 (SI), were obtained by varying the external resistance from 1 Ω to 90 kΩ. It was noticed that the $MnCo_2O_4$ NRs content in the composite can significantly affect the power generation performance. It is quite evident from the anode polarization curves that there are insignificant variations in the anode voltage for all sMFC with $MnCo_2O_4$ NRs loadings. In contrast, the variation in cathode voltage is pronounced depending on $MnCo_2O_4$ NRs loading in Vulcan XC. Fig. S7 (SI) shows the polarization and power density curves for sMFC with different catalyst loadings. The sMFC with the catalyst-free cathode produced a maximum volumetric power density ($P_{d,max}$) of 1.77 W/m^3, which increases with $MnCo_2O_4$ NRs loading. The $P_{d,max}$ is measured to be 2.68, 3.36, 4.1, and 4.22 W/m^3 for 0.05, 0.1, 0.2 and 0.4 mg/cm^2 $MnCo_2O_4$ NRs loading, respectively. A significant increase in $P_{d,max}$ is observed by increasing $MnCo_2O_4$ NRs loading up to 0.2 mg/cm^2. However, not much increase in the $P_{d,max}$ is observed for further increasing the loading to 0.4 mg/cm^2 indicating near saturation level of catalyst loading in the cathode. The gradual increase in $P_{d,max}$ can be attributed to better ORR kinetics at cathode and smaller ORR activation energy. With the increasing of the catalyst loading, more ORR active sites are available and thereby reduction kinetics is improved. One of the possible reasons that $MnCo_2O_4$ shows improved ORR property is the presence of Mn increases the Co^{2+}/Co^{3+} ratio in it and produces more electroactive centers (Restovic et al., 2002). The 0.2 mg/cm^2 of $MnCo_2O_4$ NRs is found to be the optimum loading for the highest performance-to-cost ratio of sMFC in the power generation. However, the conductivity of electrode is expected to decrease at a higher loading resulting poor electron transport. So, the linear increase in the power generation is not observed with increasing the loading. Another possible cause on the slowdown of ORR activity is low oxygen diffusion at the cathode surface on the compact catalyst layer with a higher loading.

3.4. *Influence of carbon support in the air-cathode for sMFC*

$MnCo_2O_4$ has low electrical conductivity, which is unfavorable for the fast electronic transfer during the electrocatalytic process such as ORR (Sugawara et al., 1997). Therefore, $MnCo_2O_4$ NRs must be blended with conductive carbon filler to fabricate cathode to improve the charge transport. In order to explore the suitability of carbon support for air-cathode in the sMFC, performance of $MnCo_2O_4$ NRs/Vulcan-XC was compared with m-$MnCo_2O_4$ NRs/PPy and *in situ*-$MnCo_2O_4$ NRs/PPy composites with a fixed 0.2 mg/cm^2 $MnCo_2O_4$ NRs loading. The $P_{d,max}$ obtained with $MnCo_2O_4$ NRs/Vulcan-XC, m-$MnCo_2O_4$ NRs/PPy and *in situ*-$MnCo_2O_4$ NRs/PPy in the sMFC was 4.1, 5.05 and 6.11 W/m^3, respectively (Fig. 4). The higher power generation ability of PPy supported $MnCo_2O_4$ NRs air-cathode is attributed to the low R_{ct} and higher reduction kinetics. The air-cathode with *in situ*-$MnCo_2O_4$ NRs/PPy composite performed better in terms of power generation than that of m-$MnCo_2O_4$ NRs/PPy. This is due to the good distribution of $MnCo_2O_4$ NRs in PPy matrix leading easy electron transfer between them. However, such a facile electron transfer is slow in case of m-$MnCo_2O_4$

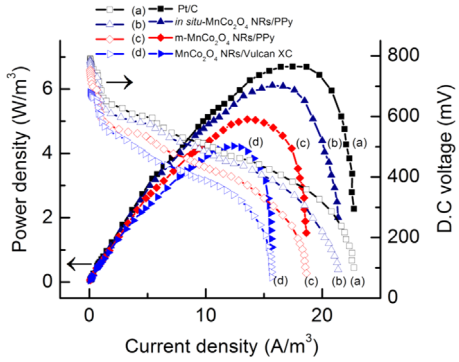

Fig. 4. Polarization plots for sMFC (power density and D.C. voltage as a function of current density) with different air-cathodes (a) Pt/C, (b) *in situ*-$MnCo_2O_4$ NRs/PPy, (c) m-$MnCo_2O_4$ NRs/PPy, and (d) $MnCo_2O_4$ NRs/Vulcan XC composites. The power density and voltage data points are presented as solid and open symbols, respectively. Fixed quantity of catalyst (0.2 g/cm^2 $MnCo_2O_4$ NRs or Pt) was loaded to different carbon supports for the comparison.

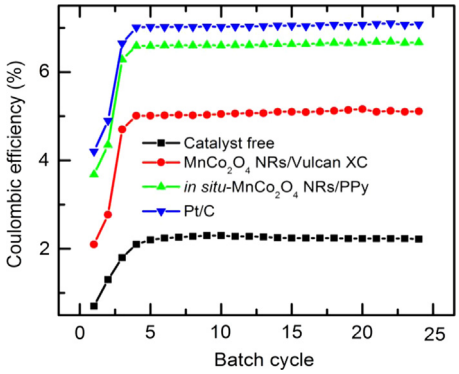

Fig. 5. Coulombic efficiency (%) profile of different air-cathodes based sMFC.

NRs/PPy composite due to poor dispersion of catalyst in the PPy matrix.

Previously, researchers have utilized PPy as support and/or ORR catalyst in different applications. Yuan et al. have used PPy/C composite as cathode catalyst in air-cathode MFC and found a better performance as compared to non-pyrolysed FePc (ORR activity was measured in 50 mM phosphate buffer solution) (Yuan et al., 2010). Electrodeposited PPy/anthraquinone-2-sulfonate (PPy/AQS) film on stainless steel mesh has been used as cathode in a membrane-less MFC (Feng et al., 2011). However, literature survey reveals that PPy/AQS composite electrode follows less efficient 2-electron ORR pathway at pH 4.3 and produces harmful HO_2^- (Zhao et al., 2011). Recently, Lu et al. reported an average 2.8 electron transfers to single oxygen molecule in 0.2 M NaCl and H_2O_2 as one of the intermediates with manganese-PPy-carbon nanotube air-cathode comprised MFC (Lu et al., 2013). Mahmoud et al. reported spinel manganese-cobalt oxide as a cathode catalyst for the sMFC and obtained a $P_{d,max}$ 138 mW/m^2 which is much lower than that obtained in the present study (420 mW/m^2 with *in situ*-$MnCo_2O_4$ NRs/PPy) (Mahmoud et al., 2011). The unique electronic structure of PPy aids in reducing the activation energy for O_2 adsorption on the composite catalyst and enhances the electron transfer which improves ORR kinetics (as supported by EIS, Fig. S5, (SI). Furthermore, the improved catalytic activity is believed to be contributed from the C–N-metal bonds formation in the composites (Liang et al., 2012). The easy processibility, high electronic and protonic conductivity of PPy as compared to Vulcan XC make it as an alternate catalyst support for several electrochemical applications. Therefore, it is important to compare the power generation ability of as-synthesized $MnCo_2O_4$ NRs/PPy composites with the benchmark Pt/C catalyst. The $P_{d,max}$ of benchmark Pt/C (6.7 W/m^3) is found to be not significantly higher than that of *in situ*-$MnCo_2O_4$ NRs/PPy composite (6.1 W/m^3) as shown in Fig. 4. This indicates that the low-cost $MnCo_2O_4$ NRs supported PPy has potential to replace expensive Pt.

3.5. Bioelectrochemical treatment and Coulombic efficiency (CE)

CE is one of the key parameters used to evaluate the capacity of MFC for converting the energy present in the organic matter into the electricity. Fig. 5 shows the CE obtained from the sMFC with different air-cathode composites. After 2 weeks of operation, the average CE of catalyst-free, $MnCo_2O_4$ NRs/Vulcan XC, *in situ*-$MnCo_2O_4$ NRs/PPy and Pt/C cathode-based sMFC was estimated to be 2.24%, 5.9%, 6.65%, and 7%, respectively. The chemical oxygen demand (COD) removal follows same trend as that of CE with the order of catalyst-free (70%) < $MnCo_2O_4$ NRs/Vulcan XC (84.4%) < *in situ*-$MnCo_2O_4$ NRs/PPy (89.8%) < Pt/C (91.2%). The $MnCo_2O_4$ NRs has shown higher CE and COD removal as compared to the catalyst-free sMFC because of better ORR. It is important to note that the sMFC with *in situ*-$MnCo_2O_4$ NRs/PPy loaded cathode shows comparable CE as that achieved with Pt/C. However, the overall CE was relatively low in spite of using pure culture of *S. putrefaciencs*. It could be due to the penetration of oxygen through the cathode because catalyst loaded conductive carbon ink was sprayed on the air facing side of the membrane without using carbon paper or cloth. The oxygen penetration from the cathode side to the anode would make the anodic operation partially aerobic and consequently, many substrates can be degraded without generating electricity. Additionally, electron transfer from anode to cathode is generally hampered by different losses which lower the power output of MFC. The electrons generated from substrate degradation need to overcome various barriers during their transportation from biocatalyst to cathode via anode, which incurs energy loss and can account under activation losses. The Tafel plot and Relative change in cathode potentials (RCCP) are generally used to measure the voltage drop and sustainability of power generation, respectively. The detail discussion on Tafel plot and RCCP is presented in the Supplementary material (SI).

4. Conclusions

In the present study, $MnCo_2O_4$ NRs are demonstrated as a potential ORR catalyst for the MFC. The sMFC performance improves with $MnCo_2O_4$ NRs loading in Vulcan XC. Furthermore, PPy is demonstrated as an alternate conducting support to Vulcan XC. The catalyst-support preparation method is found to play an important role in the performance of cathode in the sMFC with the *in situ*-$MnCo_2O_4$ NRs/PPy composite showing higher efficiency than that of m-$MnCo_2O_4$ NRs/PPy composite, which is attributed to higher interfacial contact between catalyst and PPy. The catalytic behavior of $MnCo_2O_4$ NRs based air-cathode is compared with benchmark Pt/C. The sMFC performance in term of CE and COD removal of *in situ*-$MnCo_2O_4$ NRs/PPy composite is found to be close to the benchmark Pt/C. The present work reveals that the high performance-to-cost ratio of *in situ*-$MnCo_2O_4$ NRs/PPy composite is a potential alternate to the Pt/C air-cathode for the large scale application of MFC.

Acknowledgments

This work is supported by the Department of Science and Technology, New Delhi through the Grant Indo-Korea/P-02. SK and

SP are thankful to UGC and CSIR, New Delhi, India for JRF and SRF fellowship, respectively.

Appendix A. Supplementary material

Supplementary data associated with this article can be found in the online version at http://dx.doi.org/10.1016/j.bios.2013.11.044.

References

Ahmed, J., Yuan, Y., Zhou, L., Kim, S., 2012. J. Power Sources 208, 170–175.
Carpenter, M.K., Moylan, T.E., Kukreja, R.S., Atwan, M.H., Tessema, M.M., 2012. J. Am. Chem. Soc. 134, 8535–8542.
Chen, X., Li, F., Wang, X., Sun, S., Xia, D., 2012. J. Phys. Chem. C 116, 12553–12558.
Feng, C., Wan, Q., Lv, Z., Yue, X., Chen, Y., Wei, C., 2011. Biosens. Bioelectron. 26, 3953–3957.
Guo, S., Sun, S., 2012. J. Am. Chem. Soc. 134, 2492–2495.
Hamdani, M., Singh, R.N., Chartier, P., 2010. Int. J. Electrochem. Sci. 5, 556–577.
He, Q., Li, Q., Khene, S., Ren, X., López-Suárez, F.E., Lozano-Castelló, D., Bueno-López, A., Wu, G., 2013. J. Phys. Chem. C 117, 8697–8707.
Khomenko, V.G., Barsukov, V.Z., Katashinskii, A.S., 2005. Electrochim. Acta 50, 1675–1683.
Kim, B.H., Chang, I.S., Gadd, G.M., 2007. Appl. Microbiol. Biotechnol. 76, 485–494.
Li, W.-W., Sheng, G.-P., Liu, X.-W., Yu, H.-Q., 2011. Bioresour. Technol. 102, 244–252.
Liang, Y., Wang, H., Zhou, J., Li, Y., Wang, J., Regier, T., Dai, H., 2012. J. Am. Chem. Soc. 134, 3517–3523.
Lu, M., Guo, L., Kharkwal, S., Wu, H., Ng, H.Y., Li, S.F.Y., 2013. J. Power Sources 221, 381–386.
Lu, M., Kharkwal, S., Ng, H.Y., Li, S.F.Y., 2011. Biosens. Bioelectron. 26, 4728–4732.
Luo, Y., Zhang, F., Wei, B., Liu, G., Zhang, R., Logan, B.E., 2013. Biochem. Eng. J. 73, 49–52.
Mahmoud, M., Gad-Allah, T.A., El-Khatib, K.M., El-Gohary, F., 2011. Bioresour. Technol. 102, 10459–10464.
Mohana Reddy, A.L., Rajalakshmi, N., Ramaprabhu, S., 2008. Carbon 46, 2–11.
Pandit, S., Ghosh, S., Ghangrekar, M.M., Das, D., 2012. Int. J. Hydrogen Energy 37, 9383–9392.
Raghavulu, S.V., Babu, P.S., Goud, R.K., Subhash, G.V., Srikanth, S., Mohan, S.V., 2012. RSC Adv. 2, 677.
Restovic, A., Rios, E., Barbato, S., Ortiz, J., Gautier, J.L., 2002. J. Electroanal. Chem. 522, 141–151.
Rismani-Yazdi, H., Carver, S.M., Christy, A.D., Tuovinen, O.H., 2008. J. Power Sources 180, 683–694.
Roche, I., Katuri, K., Scott, K., 2009. J. Appl. Electrochem. 40, 13–21.
Sevda, S., Dominguez-Benetton, X., Vanbroekhoven, K., De Wever, H., Sreekrishnan, T.R., Pant, D., 2013. Appl. Energy 105, 194–206.
Sugawara, M., Ohno, M., Matsuki, K., 1997. J. Mater. Chem. 7, 833–836.
Wang, L., Liang, P., Zhang, J., Huang, X., 2011. Bioresour. Technol. 102, 5093–5097.
Wang, S., Yu, D., Dai, L., 2011. J. Am. Chem. Soc. 133, 5182–5185.
Wu, Z.-S., Yang, S., Sun, Y., Parvez, K., Feng, X., Müllen, K., 2012. J. Am. Chem. Soc. 134, 9082–9085.
Xu, J., Gao, P., Zhao, T.S., 2012. Energy Environ. Sci. 5, 5333.
Yuan, X., Ding, X.-L., Wang, C.-Y., Ma, Z.-F., 2013. Energy Environ. Sci. 6, 1105.
Yuan, Y., Zhou, S., Zhuang, L., 2010. J. Power Sources 195, 3490–3493.
Zhang, X., Sun, H., Liang, P., Huang, X., Chen, X., Logan, B.E., 2011. Biosens. Bioelectron. 30, 267–271.
Zhao, F., Harnisch, F., Schröder, U., Scholz, F., Bogdanoff, P., Herrmann, I., 2005. Electrochem. Commun. 7, 1405–1410.
Zhao, S., Zhang, G., Fu, L., Liu, L., Fang, X., Yang, F., 2011. Electroanalysis 23, 355–363.
Zhou, M., Chi, M., Luo, J., He, H., Jin, T., 2011. J. Power Sources 196, 4427–4435.
Zhuang, L., Zhou, S., Wang, Y., Liu, C., Geng, S., 2009. Biosens. Bioelectron. 24, 3652–3656.
Zuo, Y., Cheng, S., Call, D., Logan, B.E., 2007. Environ. Sci. Technol. 41, 3347–3353.